Electron-ion recombination of Fe II

Sultana N. Nahar
Department of Astronomy, The Ohio State University, Columbus, Ohio 43210
(Received 20 August 1996)

A complete treatment of electron-ion recombination of $e+$Fe III$\rightarrow$Fe II employing a unified method is presented. The treatment incorporates both the radiative and dielectronic recombinations in a self-consistent manner. Total recombination rate coefficients are obtained from photoionization cross sections, and from collision strengths for dielectronic recombination calculated using the precise theory of Bell and Seaton [J. Phys. B **18**, 1589 (1985)]. Large-scale computations for both of these quantities are carried out in the close coupling approximation using the R-matrix method with an eigenfunction expansion that includes 83 states of Fe III dominated by the ground $3d^6$, and the excited $3d^5 4s$ and $3d^5 4p$ configurations. Both the total and state-specific recombination rate coefficients are obtained. Comparison of the present results with the previous ones shows considerable difference for most of the temperature regions. The present results provide accurate and self-consistent recombination rates, in the temperature range of practical applications ($T<10^5$ K), for ionization balance in photoionization models employing the detailed photoionization cross sections from the Opacity Project. [S1050-2947(97)00103-0]

PACS number(s): 34.80.Kw, 32.80.Dz, 32.80.Fb, 33.80.Eh

I. INTRODUCTION

Fe II is a complex atomic system with strong electron correlation effects that render a quantum mechanical description difficult in terms of accurate wave functions, and consequently, to calculate atomic parameters with high precision. Hence, though it is astrophysically very important, little theoretical work has been carried out [1,2] for the recombination process of $e+$Fe III$\rightarrow$Fe II. The coupled-channel approximations that aim to treat low-energy electron-ion interactions precisely have been applied to lighter atomic systems, and only recently systematic calculations have been done for a few of the iron group elements, primarily iron (e.g., Refs. [3,4]). With respect to electron-ion recombination, earlier investigations treat separately the processes of radiative recombination (RR) via the background electron-ion continuum, and the dielectronic recombination (DR) via autoionizing resonances, using different approximations that are usually valid in different energy and temperature regions. Therefore inconsistencies and inaccuracies tend to get introduced into the total rates obtained from addition of the RR and the DR rates. In the two previous works on recombination of Fe II, Woods *et al.* [1] obtained the RR rate coefficients from photoionization cross sections in the central-field and the hydrogenic approximations (these approximations do not include resonances), and DR rate coefficients from the Burgess general formula [5]. Hahn [2] obtained the DR rates from an improved empirical formula as an extension of the Burgess general formula.

The present work reports a detailed study of electron-ion recombination of Fe II. Both the total and state-specific electron-ion recombination rate coefficients are obtained employing a unified treatment [6–8]. The treatment incorporates the RR and DR in a self-consistent manner in the close coupling (CC) approximation. In previous works we have applied the treatment to ions in the second and third row elements (e.g., [8,9]) and it is being extended to large, complex ions of the iron group, such as the Fe ions (e.g., Fe III [10], Fe I ([11]). The recombination rates are presented for a wide range of temperature.

II. THEORETICAL SUMMARY AND COMPUTATIONS

The theoretical details of the unified treatment for the total electron-ion recombination rates are given in Refs. [7,8,10]. In the treatment, the infinite number of final recombined states are divided into two groups: (A) low-n bound states ranging from the ground state to excited states with $n\leqslant n_{\max}$ that are treated via photorecombination using detailed balance with photoionization in the energy range where both the background and resonant recombinations are important, and (B) recombination via high-lying resonances to high-n bound states of the $e+$ion system with $n_{\max}\leqslant n\leqslant\infty$ (i.e., DR) in the energy range where background recombination (as opposed to resonant recombination) is negligibly small. Typical choice of $n_{\max}$ is 10 (11 in a few cases). Hence the recombination rates are obtained from the partial photoionization cross sections of a large number of bound states, leaving the residual ion in the ground state, and DR collision strengths in the energy range where DR dominates; i.e., below the threshold(s) of convergence of resonances with high principal quantum number (referred to as high-n resonances). Extensive large-scale computations are carried out for the atomic data for the ion. We provide some computational details of the atomic calculations below.

Calculations are carried out in the close coupling approximation where the target or the core ion is represented by an N-electron system, and the recombined ion by an $(N+1)$-electron system. The total wave function expansion $\Psi(E)$ of the $(N+1)$-electron system for any symmetry $SL\pi$ is represented in terms of the target wave functions as

$$\Psi(E)=A\sum_i \chi_i\theta_i+\sum_j c_j\Phi_j, \qquad (2.1)$$

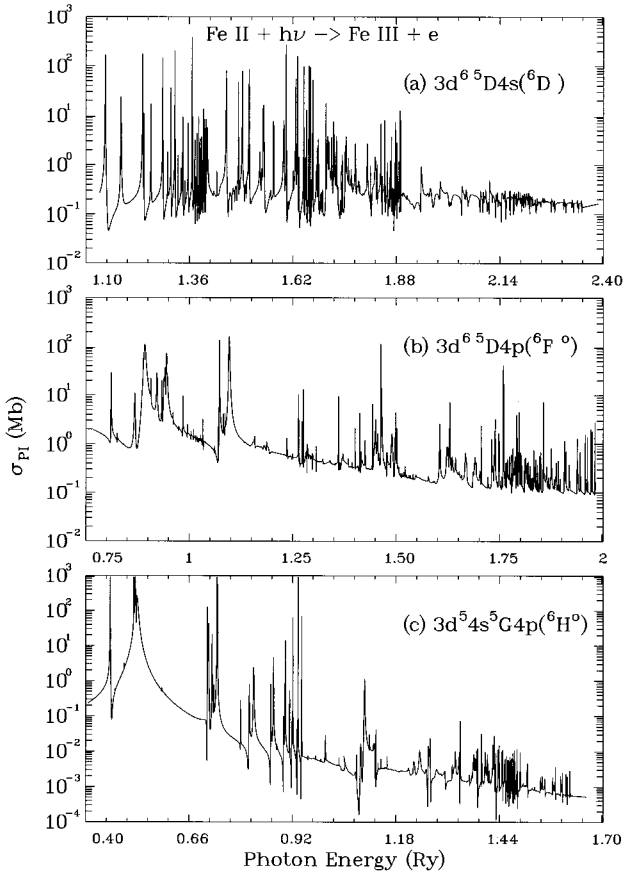

FIG. 1. Partial photoionization cross sections $\sigma_{\rm PI}$ of the (a) ground state ^6D and excited states (b) $3d^5 4s\,^5G 4p(^6H^o)$ and (c) $3d^6\,^5D 4p(^6F^o)$ of Fe II.

where χ_i is the target wave function in a specific state $S_i L_i \pi_i$ and θ_i is the wave function for the $(N+1)$th electron in a channel labeled as $S_i L_i \pi_i k_i^2 l_i (SL\pi)$, k_i^2 being its kinetic energy. Φ_j's are the correlation functions of the $(N+1)$-electron system that account for short range correlation and the orthogonality between the continuum and the bound orbitals. Present work on photoionization cross sections $\sigma_{\rm PI}$ of the group (A) bound states, and collision strengths of DR, Ω(DR), of the group (B) states, employs an extensive eigenfunction expansion of 83 states [3] which includes important correlation effects. For example, the expansion for Fe II includes most of the dominant terms from the ground $3d^6$, excited $3d^5 4s$, and $3d^5 4p$ configurations. Observed energies for the target states are used to determine the accurate positions of the resonances.

Some important features of the partial photoionization cross sections and DR collision strengths relevant to their respective contributions to the total recombination rate coefficients will be illustrated blow.

A. Low-*n* states: Partial photoionization cross sections

For the group (A) low-n bound states, the partial photoionization cross sections $\sigma_{\rm PI}$ leaving the core in the ground state are obtained for each bound state. The autoionizing resonances are included where they are resolved in detail [7]. Computations are carried out employing the R-matrix codes from the Opacity Project [12] and the Iron Project [13], and a modified version of a program to compute bound-free cross sections, STGBF [8]. The present calculations obtain 525 bound states that couple to the ground state $3d^6(^5D)$ of the core ion Fe III, of which 195 are sextets and 330 are quartets. However, the total number of such bound states observed is 158, 40 sextets and 118 quartets. Partial photoionization cross sections of all the 525 bound states of Fe II are calculated and included in the total $\alpha_R(T)$.

Although the 83-state eigenfunction expansion of Fe III of Nahar and Pradhan [3] is used for most of the present computations, it was found necessary to reduce the size of the expansion for computations of partial photoionization cross sections for the quartet states of Fe II which required far too much computational time on the Cray Y-MP. Some highly excited even parity states, such as ^5F (27th target state) and some weakly coupled states to the ground state, such as $^5H^o$ (47th target state), are omitted in the reduced expansion; the highest state included is the 60th target state, $3d^5 4p(^5P^o)$ [3]. This still ensures inclusion of almost all contributing series of autoionizing resonances, except from the highest excited states $^5F^o$ (80th state) and $^5D^o$ (82nd state) for dipole allowed transitions from the ^5D ground state. Comparison of the present partial cross sections with

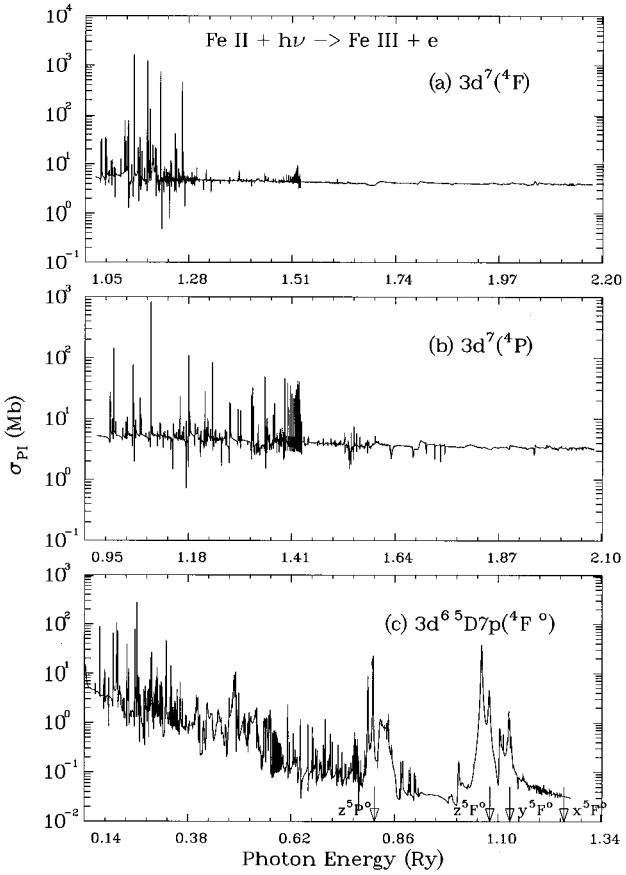

FIG. 2. Partial photoionization cross sections $\sigma_{\rm PI}$ of the metastable states (a) $3d^7(^4F)$, (b) $3d^7(^4P)$, and (c) excited $3d^6\,^5D 7p(^4F^o)$ state of Fe II. (c) illustrates the PEC resonances with the arrows pointing the energy positions for PEC's at thresholds $3d^5 4p(z^5P^o)$, $3d^5 4p(z^5F^o, z^5D^o, y^5P^o)$, $3d^5 4p(y^5F^o, y^5D^o, x^5P^o)$, and $3d^5 4p(x^5F^o, x^5D^o)$ for dipole allowed transitions. The states within parentheses are treated as degenerate in the computations.

the earlier total photoionization cross sections of Fe II [3] shows no significant loss of resonances and only a slightly lower background as expected from the difference of total and the partial cross sections. The contribution to DR from all dipole transitions in the target expansion is included, as explained later.

The recombination cross sections $\sigma_{\rm RC}$ are obtained from the $\sigma_{\rm PI}$ through the Milne relation (detailed balance). The recombination rate coefficients are obtained on averaging $\sigma_{\rm RC}(T)$ over the Maxwellian electron distribution, at a given temperature T, using the code RECOMB [10]. The recombination rate coefficients thus obtained from the partial photoionization cross sections of the low-n bound states incorporate both the RR and the DR processes and provide total photorecombination rates. Although the ground state of Fe II, $3d^64s(^6D)$, is an important contributor, it is not the dominant contributor to the recombination rates. The reason can be explained from the detailed structures of the cross sections presented in Figs. 1 and 2, discussed below.

Figure 1 presents the photoionization cross sections of the ground state, (a) $3d^6\ ^5D4s(^6D)$, and two dominant contributing states, (b) $3d^6\ ^5D4p(^6F^o)$, and (c) $3d^54s^5G4p(^6H^o)$, of Fe II. The ground ^6D state shows extensive resonances indicating high autoionization rates. However, the excited $^6F^o$ state shows more enhanced effective background cross sections than the ground state and hence contributes considerably more to the recombination rates than the ground state. The excited $^6H^o$ state dominates the recombination because of large and wide resonances in the low-energy region.

Figure 2 presents the photoionization cross sections of two metastable states (a) $3d^7(^4F)$, (b) $3d^7(^4P)$, and (c) excited $3d^6\ ^5D7p(^4F^o)$ state. Both of the metastable states are dominant contributors to the recombination rates because of their background cross sections. Although the autoionizing resonances do not continue as energy increases, for these states the background cross sections remain high, contributing significantly to the recombination rates. Figure 2(c) illustrates the PEC (photoexcitation of core) resonances in the cross sections of highly excited Rydberg bound states. The PEC resonances in the photoionization cross sections represent the inverse of the DR process and manifest themselves through excitation of the core due to a dipole allowed transition from the ground state, while the outer electron remains a spectator. These resonances are wider than the Rydberg resonances and enhance the cross sections, often by orders of magnitude.

The PEC resonances are more prominent for excited states with one electron in a Rydberg state, and the energy behavior of the cross section deviates considerably from the hydrogenic form usually assumed for the photoionization cross section of such states. Figure 2(c) shows the cross sections of such an excited state, $3d^6\ ^5D7p(^4F^o)$, where the arrows point to the threshold energies of the PEC resonances at $3d^54p(z^5P^o)$, $3d^54p(z^5F^o,z^5D^o,y^5P^o)$, $3d^54p(y^5F^o,y^5D^o,x^5P^o)$, and $3d^54p(x^5F^o,x^5D^o)$, corresponding to dipole allowed transitions from the ground ^6D state. The target states within the parentheses are narrowly spaced and are treated as degenerate [3]. The first three PEC resonances are quite pronounced in the figure, while the last one is not so obvious due to weaker coupling.

B. High-n states: Collision strengths for dielectronic recombination

The recombination of group (B) states, $n_{\rm max}<n\leqslant\infty$, is dominated by DR since the number of Rydberg series of states belonging to the target thresholds increases as ν^3 and the autoionization rate decreases as ν^{-3}, where ν is the effective quantum number of the Rydberg series. We calculate the collision strengths for DR for these states employing the theory of DR by Bell and Seaton [14,7]. Calculations are carried out in the close coupling approximation using the same 83-CC eigenfunction expansion that is used for the partial photoionization cross sections. The computations of the DR collision strengths are carried out employing the extended code STGFDR of STGF [7]. A few details are given below.

The calculations of the DR probability for $e+{\rm Fe\ III}\rightarrow{\rm Fe\ II}$ involve nine dipole allowed transitions from the ^5D ground state out of the 83 states in the expansion. These transitions along with their radiative transition probabilities (A values) are given in Table I. The A values are taken from the 49-CC calculations of Fe III f values [4]. Some of the states for dipole allowed transitions are treated as degenerate when they are closely spaced in energy. The threshold energies are taken to be $3d^54p(z^5P^o)$ at 0.818 Ry, $3d^54p(z^5F^o,z^5D^o,y^5P^o)$ at 1.081 Ry, $3d^54p(y^5F^o,y^5D^o,x^5P^o)$ at 1.127 Ry, and $3d^54p(x^5F^o,x^5D^o)$ at 1.257 Ry. Thus the value of Ω(DR) at various thresholds, except at the first threshold with only one target state, corresponds to the sum of contributions from the channels belonging to all the degenerate states at each threshold.

The Ω(DR) for (e^-,Fe III) are obtained in two forms: (i) with detailed resonance profiles, and (ii) averaged over the resonances. Both forms are presented in Fig. 3 where the dotted curve corresponds to the detailed Ω(DR), and the solid curve to the resonance averaged values. The common features of DR are observed in the figure: the resonances become denser with increasing n along a Rydberg series converging to the excited states (marked by the arrows); the background rises as the energy approaches these thresholds. The resonance averaged solid curve peaks at the thresholds. The trapped electron flux in the closed channels below the thresholds is released as the channels open up at the thresholds and DR contribution goes to zero. The peak values of the $\langle\Omega({\rm DR})\rangle$ at the thresholds are given in Table I. For the calculation of the present total recombination rates the averaged Ω(DR), rather than the detailed, is used as it is more accurate for numerical integration.

Independent electron-ion scattering calculations are also carried out for the electron impact excitation collision (EIE) strengths Ω(EIE) at the threshold energies for the dipole allowed transitions in the core ion. For Fe III, the same 83-state eigenfunction expansion (as in the DR and the photoionization calculations) is employed in the CC calculations for Ω(EIE). This provides a few checks for the values of DR collision strengths. The convergence of the R-matrix basis set is checked in terms of the multipole potential contributions [7]. The present theory of DR collision strengths, based on multichannel quantum defect theory, neglects the contribution of higher order (nondipole) multipole potentials.

TABLE I. Transition probabilities A_{ji} and collision strengths of EIE (with IPERT=0 and 1) and of DR at the thresholds for dipole allowed transitions in Fe III. For a threshold with degenerate states, the last line corresponds to the sum of collision strengths. Numbers in brackets represent powers of ten.

Transition	A_{ji} (a.u.)	$\langle\Omega(\mathrm{DR})\rangle$	$\Omega(\mathrm{EIE})_0$	$\Omega(\mathrm{EIE})_1$
$a^5D^e \rightarrow z^5P^o$	1.08[−8]	11.70	11.50	9.12
$a^5D^e \rightarrow z^5D^o$	1.71[−12]	↓	0.962	1.03
$a^5D^e \rightarrow y^5P^o$	1.96[−8]	↓	7.59	7.00
$a^5D^e \rightarrow z^5F^o$	1.58[−8]	↓	11.09	10.11
		7.69	19.64	18.14
$a^5D^e \rightarrow y^5D^o$	1.76[−8]	↓	5.72	5.40
$a^5D^e \rightarrow x^5P^o$	2.70[−9]	↓	0.598	5.88
$a^5D^e \rightarrow y^5F^o$	3.63[−9]	↓	2.63	2.54
		7.51	8.95	8.52
$a^5D^e \rightarrow x^5D^o$	1.35[−8]	↓	2.65	2.66
$a^5D^e \rightarrow x^5F^o$	2.89[−9]	↓	1.33	1.33
		3.08	3.98	3.98

However, this can be compensated for through a proper choice of the size of the R-matrix boundary and the number of terms in the R-matrix basis set. The comparison between the values of excitation collision strengths Ω(EIE) obtained using a parameter IPERT=0 (exclusion of multipole potentials) and IPERT=1 (inclusion of multipole potentials), indicates the significance of the multipole potential contributions, as explained in Nahar and Pradhan [7]. For the present case, the values of Ω(EIE) with IPERT=0 and 1 are presented in Table I. Except for the first transition, the values of

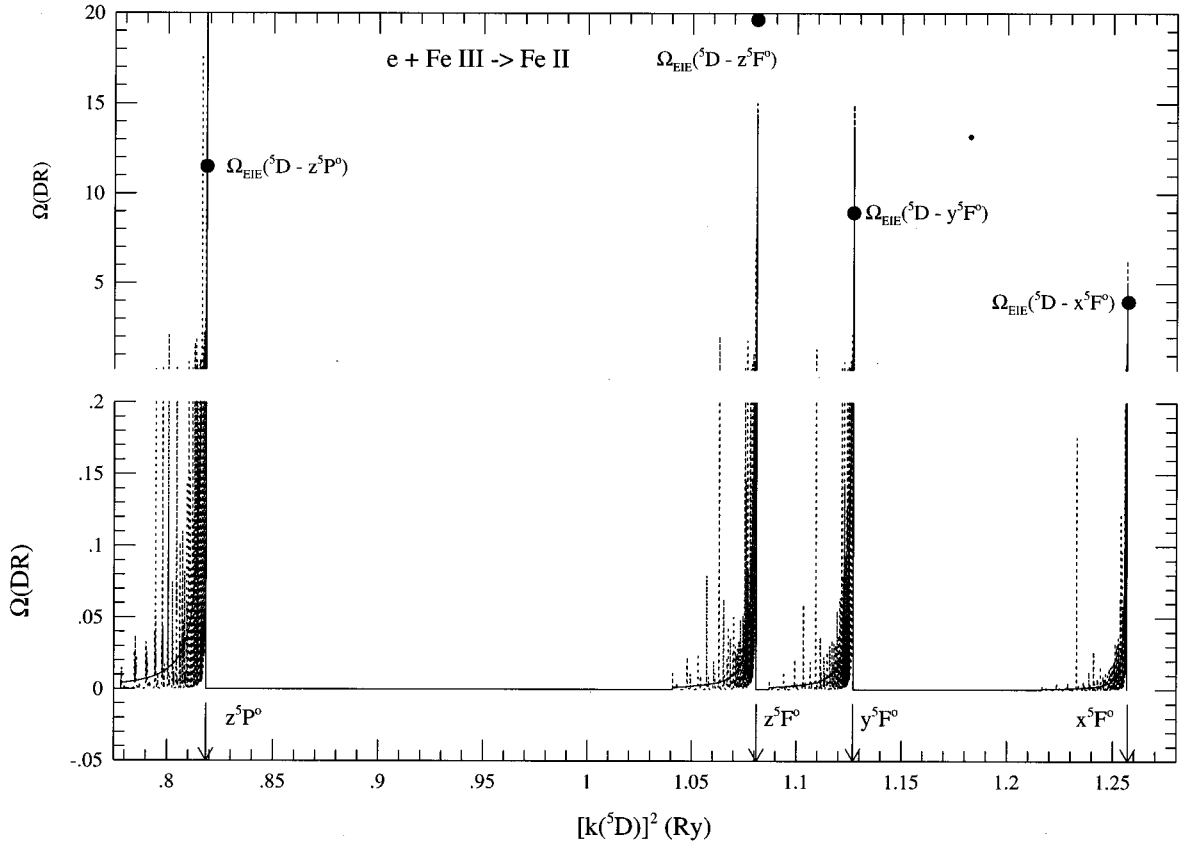

FIG. 3. DR collision strength Ω(DR) for the recombination of e+Fe III→Fe II: (i) detailed with resonances (dotted curves) and (ii) resonance averaged (solid curves). DR calculations start at effective quantum number $\nu=10$ of the Rydberg series of states belonging to the thresholds (pointed by the arrows) for dipole allowed transitions of the ground ^5D state of Fe III. Only one state is specified at the thresholds with degenerate states (explained in text). The filled circles are the values of excitation collision strength Ω(EIE); at the thresholds with degenerate states, they represent the total sum of Ω(EIE).

TABLE II. Total recombination rate coefficients $\alpha_R(T)$ in units of $cm^3\,s^{-1}$, for the recombination of $e+$Fe III$\rightarrow$Fe II at various temperatures T (K). Numbers in brackets represent powers of ten.

$\log_{10}T$	α_R	$\log_{10}T$	α_R	$\log_{10}T$	α_R
1.0	1.23[−10]	3.1	6.20[−12]	5.2	3.34[−12]
1.1	1.07[−10]	3.2	5.57[−12]	5.3	2.82[−12]
1.2	9.34[−11]	3.3	5.07[−12]	5.4	2.31[−12]
1.3	8.13[−11]	3.4	4.68[−12]	5.5	1.84[−12]
1.4	7.06[−11]	3.5	4.41[−12]	5.6	1.43[−12]
1.5	6.13[−11]	3.6	4.25[−12]	5.7	1.10[−12]
1.6	5.32[−11]	3.7	4.18[−12]	5.8	8.28[−13]
1.7	4.61[−11]	3.8	4.14[−12]	5.9	6.19[−13]
1.8	3.98[−11]	3.9	4.11[−12]	6.0	4.58[−13]
1.9	3.45[−11]	4.0	4.02[−12]	6.1	3.37[−13]
2.0	2.97[−11]	4.1	3.85[−12]	6.2	2.47[−13]
2.1	2.56[−11]	4.2	3.63[−12]	6.3	1.77[−13]
2.2	2.21[−11]	4.3	3.42[−12]	6.4	1.29[−13]
2.3	1.90[−11]	4.4	3.31[−12]	6.5	9.34[−14]
2.4	1.63[−11]	4.5	3.38[−12]	6.6	6.74[−14]
2.5	1.40[−11]	4.6	3.61[−12]	6.7	4.87[−14]
2.6	1.21[−11]	4.7	3.93[−12]	6.8	3.51[−14]
2.7	1.04[−11]	4.8	4.18[−12]	6.9	2.54[−14]
2.8	9.03[−12]	4.9	4.26[−12]	7.0	1.83[−14]
2.9	7.91[−12]	5.0	4.13[−12]		
3.0	6.97[−12]	5.1	3.80[−12]		

Ω(EIE) with IPERT=0 and 1 agree with each other in less than 10%, indicating an adequate convergence is achieved.

Another check is carried out through comparison of the value of $\langle\Omega(\mathrm{DR})\rangle$ with that of Ω(EIE) (with IPERT=0) at each threshold. Agreement between the two numbers indicates conservation of flux, such that the trapped electron flux due to resonances below a threshold equals that released due to excitation at the threshold energy. The filled circles in Fig. 3 represent the excitation collision strengths Ω(EIE) at the excited thresholds (the values are given in Table I). At thresholds with degenerate states the sum of Ω(EIE) values for the states are compared to the value of Ω(DR). As seen in Table I, the agreement between the values of $\langle\Omega(\mathrm{DR})\rangle$ and Ω(EIE) at the first threshold indicates that conservation condition of the flux is satisfied. However, at the other thresholds, differences can be seen between the peak values of $\langle\Omega(\mathrm{DR})\rangle$ and of Ω(EIE), the largest difference being at the second threshold. Several points can be made to explain the differences. Ω(DR) and Ω(EIE) are obtained from two different approaches, with coupling of *closed* channels for the former case and of *open* channels for the latter case. With the exception of the first threshold, each threshold corresponds to a few degenerate states. Such treatment of degeneracy can affect the strength of interference among the coupling channels, particularly for a complex ion such as Fe II with a large number of associated channels, more than for comparatively smaller ions [9], leading to a large difference between the two numbers. The existence of resonances in the EIE collision strengths very close to the threshold energy region (for any of the degenerate states) will also cause differences between the two collision strengths for DR and EIE at that threshold.

For the high-n group (B) states, recombination via the nonresonant background is negligible at high energies and temperatures, but is considerable for low electron energies at very low temperatures. As we aim to calculate total $e+$ion recombination rate coefficients valid in all temperature ranges, we include this contribution in the total $\alpha_R(T)$ through a ''top-up'' scheme using hydrogenic approximation for the high-n photoionization cross sections, as explained in Nahar [10].

III. RESULTS AND DISCUSSIONS

Total recombination rate coefficients $\alpha_R(T)$ are obtained for the recombination process $e+$Fe III$\rightarrow$Fe II, employing a unified treatment for a wide range of temperatures, $1\leqslant\log_{10}T\leqslant7$. Values of $\alpha_R(T)$ are obtained at a fine temperature mesh of $\Delta\log_{10}T=0.1$ for easy interpolation at any temperature. The numerical values of $\alpha_R(T)$ are provided in Table II and are plotted in Fig. 4 (the solid curve). The curve exhibits the general pattern of the total electron-ion recombination rate coefficients $\alpha_R(T)$, as discussed in previous works [8]: at low temperature the rate is high owing to background continuum recombination to many high-n states, decreasing with temperature to a minimum value just before resonant recombination (DR) becomes dominant and gives rise to the high-T DR bump, which for Fe II lies at about $\log_{10}(T)=4.8$ K. After the high-T bump, the recombination rate decreases smoothly. In addition to the prominent high-T DR bump, the α_R(Fe II) also exhibits a slight low-T bump (seen for many other ions [8]) owing to low-energy autoionizing resonances in the cross sections leading to recombination to the low-n bound states. The present recombination

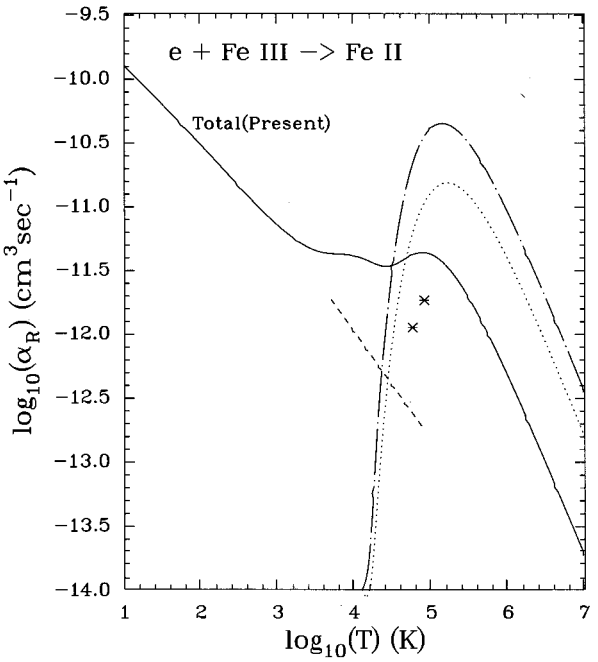

FIG. 4. Total recombination rate coefficients $\alpha_R(T)$ (solid curve) for Fe II of the present work. The dashed curve corresponds to RR rates and chain-dashed curve to DR rates by Woods *et al.* [1], the asterisks to DR rates by Hahn [2], and the dotted curve to DR rates by Arnaud and Raymond [16].

rates together with the total photoionization cross sections of the ground state of Fe II [3] provide a complete and self-consistent set of data for accurate calculations of ionization balance under photoionization equilibrium.

The present $\alpha_R(T)$ for Fe II differs considerably from the earlier rates. Comparison of the present *total* α_R (solid curve) in Fig. 4 is made with the earlier RR rates (dashed curve) and the DR rates (dot-dashed curve) of Woods *et al.* [1], and DR rates (asterisks) of Hahn [2]. The two earlier rates for RR and DR can be summed to get an estimate of the total rates. The low-T values of Woods *et al.*, valid over a small T range, underestimate the recombination rate significantly, up to a factor of 5. One reason for this is that their work does not include any resonance contributions at low energies. Their DR rates at high T obtained using Burgess's general formula [5] (BGF) are considerably higher. BGF does not take account of the extensive radiative and autoionization couplings and interference effects between channels of all relevant excited states, principally autoionization into lower excited states (as noted by Jacobs *et al.* [15]), and is therefore not likely to be accurate for the complicated case of Fe II where such coupling effects are strong. The present rates at $T>10^5$ K may be higher due to contributions from higher target states not included in the CC expansion, and resulting bound states, but should still be considerably lower than the BGF. The DR rate coefficients (asterisks) by Hahn [2] are much lower than the present values (some uncertainty is introduced from reading off the two values from the curves in Ref. [2]). Fe II is one of the ions for which accurate atomic data were not available for Hahn's empirical formula. Arnaud and Raymond [16] generated another fitting formula for the DR rates (dotted curve) by scaling the values of Woods *et al.* and of Hahn; their values lie in between the two rates, but still higher than the present values.

These are detailed calculations for electron-ion recombination of Fe II. The values of $\alpha_R(T)$ should be accurate to within 10–30 % for most of the temperature range of practical importance, up to an excitation temperature of over 10^5 K corresponding to the highest target state in the CC expansion. The estimate of accuracy is based on the general accuracy of the CC method for photoionization cross sections and electron scattering and DR collision strengths. The principal result of this work is that at astrophysical temperatures relevant to Fe II, around 10^4 K, the dominant recombinations are through low-energy resonances and background, i.e., low-T DR and RR, where the present rates should be accurate and differ considerably from the approximate data heretofore available.

The high-temperature rates ($T>10^5$ K), although not of much practical importance, are given for completeness, but are more uncertain due to possible recombinations via bound states formed with the omitted target states ($3d^5 4d$ and higher). The number of such states in near-neutral systems is not large as these entail two excited bound electrons, one in an excited target state and one in a Rydberg state belonging to that state. Also, the contribution of these highly excited states to high-temperature rates is small because the DR collision strengths decrease with increasing energy and n, autoionization into lower coupled excited states, weaker PEC resonances, and exponential Maxwellian damping. We further note that with a large target expansion, the background cross sections of comparatively highly excited states show relatively little resonance structure long before the highest target threshold; for example, the PEC's decrease in height and width considerably after only the first few thresholds. Hence the extrapolation as described in Ref. [7] should represent a good approximation for the background and the uncertainty introduced by not including the resonances due to target states beyond the highest target threshold may not have affected the rates considerably. Nonetheless, for more highly ionized ions than Fe II there may well be a significant contribution from highly excited target states.

Table III presents the state-specific, partial recombination rate coefficients of dominant bound states of the sextet and quartet symmetries of group (A), at four temperatures: $\log_{10}T=2.0$, 3.0, 3.7, and 4.0. They are listed in order of their percentage contributions to the total $\alpha_R(T)$ at these temperatures. Both the order and the amount of contributions of the states vary with temperature because of resonance structures in the photoionization cross sections for these states, as discussed in Sec. II. The rates presented should be equal to the total state-specific recombination rate coefficient at the specified temperatures since the high-n DR contribution does not dominate until about 16 000 K. There may be some uncertainty in the rates at very low temperatures where they are sensitive to both the position and the resolution of the near-threshold resonances.

It may be noted that the present large-scale computational work has yielded partial and total photoionization cross sections for all of the 525 low-lying ($n\leqslant 10$) bound states of Fe II. The complete work on photoionization and recombination of Fe II required an estimated 225 CPU hours on the Cray Y-MP.

TABLE III. State selective recombination rate coefficients (in units of $cm^3\ s^{-1}$) at four temperatures, $T=100$, 1000, 5012, and 10 000 K, of the first 20 dominant contributing states from sextet and quartet symmetries. An asterisk indicates that the state cannot be indentified. A value of $a[-b]$ for α_R means $a\times10^{-b}$.

100 K		1000 K		5012 K		10 000 K	
State	α_R	State	α_R	State	α_R	State	α_R
$3d^6\,^5D^e4p\ ^6D^o$	2.68[−13]	$3d^6\,^5D^e4s\ ^6D^e$	1.63[−13]	$3d^5 4s^5G^e4p\ ^6H^o$	1.20[−13]	$3d^5 4s^5G^e4p\ ^6H^o$	1.99[−13]
$3d^6\,^5D^e4p\ ^6F^o$	2.48[−13]	$3d^5 3p^2\ ^6D^e$	1.15[−13]	$3d^5 4s^5G^e4p\ ^6G^o$	1.05[−13]	$3d^5 4s^5G^e4p\ ^6G^o$	1.60[−13]
$3d^6\,^5D^e4f\ ^6H^o$	1.03[−13]	$3d^6\,^5D^e4p\ ^6D^o$	8.13[−14]	$3d^5 4s^5S^e4p\ ^6P^o$	9.90[−14]	$3d^5 4s^5G^e4p\ ^6F^o$	1.30[−13]
$3d^6\,^5D^e4p\ ^6P^o$	1.01[−13]	$3d^6\,^5D^e4p\ ^6F^o$	7.55[−14]	$3d^6\,^5D^e4s\ ^6D^e$	9.41[−14]	$3d^5 4s^5S^e4p\ ^6P^o$	8.72[−14]
$3d^6\,^5D^e5p\ ^6F^o$	1.00[−13]	$3d^5 4s^7S^e4p\ ^6P^o$	4.43[−14]	$3d^5 4s^5G^e4p\ ^6F^o$	7.89[−14]	$3d^6\,^5D^e4p\ ^6F^o$	7.06[−14]
$3d^6\,^5D^e5p\ ^6D^o$	9.94[−14]	$3d^6\,^5D^e4p\ ^6P^o$	4.35[−14]	$3d^5 4p^2\ ^6D^e$	6.76[−14]	$3d^6\,^5D^e4p\ ^6D^o$	6.78[−14]
$3d^6\,^5D^e4f\ ^6G^o$	9.14[−14]	$3d^5 4s^7S^e4d\ ^6D^e$	3.58[−14]	$3d^6\,^5D^e4p\ ^6D^o$	5.29[−14]	$3d^5 4s^5P^e4p\ ^6D^o$	6.09[−14]
$3d^6\,^5D^e5f\ ^6H^o$	9.13[−14]	$3d^6\,^5D^e5d\ ^6D^e$	3.49[−14]	$3d^6\,^5D^e4p\ ^6F^o$	5.06[−14]	$3d^5 4s^5D^e4p\ ^6F^o$	5.86[−14]
$3d^6\,^5D^e6p\ ^6F^o$	8.17[−14]	$3d^5 4s^5S^e4p\ ^6P^o$	3.24[−14]	$3d^6\,^5D^e4p\ ^6P^o$	3.57[−14]	$3d^6\,^5D^e4s\ ^6D^e$	5.84[−14]
$3d^6\,^5D^e5f\ ^6G^o$	7.86[−14]	$3d^6\,^5D^e4f\ ^6H^o$	3.13[−14]	$3d^5 4s^7S^e4p\ ^6P^o$	3.23[−14]	$3d^5 4p^2\ ^6D^e$	3.96[−14]
$3d^5 4s^5S^e4p\ ^6P^o$	7.09[−14]	$3d^6\,^5D^e5p\ ^6D^o$	3.10[−14]	$3d^5 4s^7S^e4d\ ^6D^e$	2.35[−14]	$3d^6\,^5D^e4p\ ^6P^o$	3.25[−14]
$3d^6\,^5D^e4f\ ^6F^o$	6.93[−14]	$3d^6\,^5D^e5p\ ^6F^o$	3.08[−14]	$3d^6\,^5D^e5p\ ^6F^o$	2.05[−14]	$3d^5 4s^5D^e4p\ ^6D^o$	2.89[−14]
$3d^6\,^5D^e6f\ ^6H^o$	6.74[−14]	$3d^5 4s^7S^e5p\ ^6P^o$	2.95[−14]	$3d^6\,^5D^e5d\ ^6D^e$	1.90[−14]	$3d^6\,^5D^e5p\ ^6D^o$	2.64[−14]
$3d^6\,^5D^e6p\ ^6D^o$	6.53[−14]	$3d^6\,^5D^e4f\ ^6G^o$	2.79[−14]	$3d^5 4s^5P^e4p\ ^6D^o$	1.83[−14]	$3d^6\,^5D^e5p\ ^6F^o$	2.63[−14]
$3d^6\,^5D^e5f\ ^6F^o$	6.06[−14]	$3d^6\,^5D^e5f\ ^6H^o$	2.78[−14]	$3d^5 4s^7S^e5p\ ^6P^o$	1.76[−14]	$3d^5 4s^7S^e4p\ ^6P^o$	2.54[−14]
$3d^6\,^5D^e6f\ ^6G^o$	5.76[−14]	$3d^6\,^5D^e6p\ ^6F^o$	2.53[−14]	$3d^6\,^5D^e5p\ ^6D^o$	1.74[−14]	$3d^5 4s^5P^e4p\ ^6P^o$	2.38[−14]
$3d^6\,^5D^e4s\ ^6D^e$	5.57[−14]	$3d^6\,^5D^e5f\ ^6G^o$	2.40[−14]	$3d^5 4s^5D^e4p\ ^6F^o$	1.55[−14]	$3d^6\,^5D^e5p\ ^6P^o$	2.26[−14]
$3d^5 4s^5G^e4p\ ^6F^o$	5.45[−14]	$3d^6\,^5D^e4f\ ^6F^o$	2.11[−14]	$3d^6\,^5D^e4f\ ^6H^o$	1.21[−14]	$3d^5 4s^5D^e4p\ ^6P^o$	2.07[−14]
$3d^6\,^5D^e7p\ ^6F^o$	5.17[−14]	$3d^6\,^5D^e6f\ ^6H^o$	2.05[−14]	$3d^5 4s^5P^e4p\ ^6P^o$	1.17[−14]	$3d^5 4s^7S^e4d\ ^6D^e$	1.72[−14]
$3d^6\,^5D^e5d\ ^6G^e$	5.16[−14]	$3d^6\,^5D^e6p\ ^6D^o$	2.02[−14]	$3d^6\,^5D^e4f\ ^6G^o$	1.08[−14]	$3d^5 4s^5P^e4p\ ^6S^o$	1.42[−14]
Sum=	1.87[−12]		9.15[−13]		9.02[−13]		1.17[−12]
Total=	2.97[−11]		6.97[−12]		4.18[−12]		4.02[−12]
% contribution=	6%		13%		22%		29%
$3d^7\ ^4F^e$	9.05[−13]	$3d^7\ ^4F^e$	3.16[−13]	$3d^7\ ^4F^e$	2.32[−13]	$3d^7\ ^4F^e$	2.27[−13]
$3d^6\,^3G^e4p\ ^4F^o$	4.70[−13]	$3d^7\ ^4P^e$	1.00[−13]	$3d^5 4s^2\ ^4F^e$	1.52[−13]	$3d^5 4s^2\ ^4F^e$	1.92[−13]
$3d^7\ ^4P^e$	3.13[−13]	$3d^6\,^5D^e4p\ ^4D^o$	7.75[−14]	$3d^6\,^5D^e4p\ ^4D^o$	5.97[−14]	$3d^5 4s^5G^e4p\ ^4F^o$	7.47[−14]
$3d^6\,^5D^e4p\ ^4D^o$	2.73[−13]	$3d^6\,^3G^e4p\ ^4F^o$	6.81[−14]	$3d^7\ ^4P^e$	5.90[−14]	$3d^6\,^5D^e4p\ ^4F^o$	5.97[−14]
$3d^6\,^3G^e4p\ ^4G^o$	2.54[−13]	$3d^6\,^5D^e4p\ ^4F^o$	6.24[−14]	$3d^6\,^3F^e4p\ ^4G^o$	5.85[−14]	$3d^6\,^5D^e4p\ ^4D^o$	5.65[−14]
$3d^6\,^5D^e4p\ ^4F^o$	1.92[−13]	$3d^6\,^5D^e4p\ ^4P^o$	4.17[−14]	$3d^6\,^5D^e4p\ ^4F^o$	5.83[−14]	$3d^5 4s^5D^e4p\ ^4F^o$	5.41[−14]
$3d^6\,^5D^e4p\ ^4P^o$	1.32[−13]	$3d^6\,^3G^e4p\ ^4G^o$	3.67[−14]	$3d^6\,^3F^e4p\ ^4F^o$	5.71[−14]	$3d^6\,^3P^e4p\ ^4D^o$	5.29[−14]
$3d^6\,^3G^e5p\ ^4F^o$	9.44[−14]	$3d^6\,^5D^e5p\ ^4F^o$	2.64[−14]	$3d^6\,^3P^e4p\ ^4D^o$	4.41[−14]	$3d^5 4s^5G^e4p\ ^4H^o$	5.29[−14]
$3d^6\,^5D^e5p\ ^4D^o$	9.01[−14]	$3d^6\,^5D^e5p\ ^4D^o$	2.53[−14]	$3d^5 4s^5D^e4p\ ^4F^o$	4.22[−14]	$3d^7\ ^4P^e$	4.89[−14]
$3d^6\,^5D^e5p\ ^4F^o$	8.77[−14]	$3d^5 4s^2\ ^4D^e$	2.21[−14]	$3d^6\,^3H^e4d\ ^4H^e$	3.44[−14]	$3d^6\,^3F^e4s\ ^4F^e$	4.89[−14]
$3d^6\,^5D^e4f\ ^4H^o$	7.01[−14]	$3d^6\,^5D^e4f\ ^4H^o$	2.13[−14]	$3d^6\,^3F^e4p\ ^4D^o$	3.36[−14]	$3d^6\,^3F^e4p\ ^4G^o$	4.59[−14]
$3d^6\,^5D^e4f\ ^4G^o$	6.01[−14]	$3d^6\,^3H^e4d\ ^4H^e$	1.84[−14]	$3d^6\,^5D^e4p\ ^4P^o$	3.32[−14]	$3d^6\,^3F^e4p\ ^4G^o$	4.49[−14]
$3d^6\,^5D^e4d\ ^4G^e$	6.00[−14]	$3d^5 4s^2\ ^4F^e$	1.82[−14]	$3d^5 4s^5D^e4p\ ^4D^o$	3.32[−14]	$3d^6\,^3F^e4p\ ^4F^o$	4.34[−14]
$3d^6\,^3H^e4p\ ^4G^o$	5.99[−14]	$3d^6\,^5D^e4d\ ^4G^e$	1.82[−14]	$3d^6\,^3H^e4p\ ^4G^o$	3.28[−14]	$3d^6\,^3H^e4s\ ^4H^e$	4.33[−14]
$*\ ^4F^o$	5.90[−14]	$3d^6\,^5D^e4f\ ^4G^o$	1.80[−14]	$3d^5 4s^5G^e4p\ ^4F^o$	3.20[−14]	$3d^5 4s^5D^e4p\ ^4D^o$	3.99[−14]
$3d^6\,^5D^e5f\ ^4G^o$	5.78[−14]	$3d^6\,^5D^e6p\ ^4F^o$	1.64[−14]	$3d^6\,^5D^e4s\ ^4D^e$	3.12[−14]	$3d^6\,^5D^e4s\ ^4D^e$	3.86[−14]
$3d^6\,^5D^e6p\ ^4F^o$	5.23[−14]	$3d^6\,^3H^e5d\ ^4H^e$	1.63[−14]	$3d^6\,^3H^e5d\ ^4H^e$	3.05[−14]	$3d^6\,^3H^e4p\ ^4G^o$	3.55[−14]
$3d^6\,^5D^e5d\ ^4G^e$	5.12[−14]	$3d^6\,^5D^e5f\ ^4G^o$	1.62[−14]	$3d^6\,^3F^e4s\ ^4F^e$	3.00[−14]	$3d^6\,^3G^e4s\ ^4G^e$	3.37[−14]
$3d^6\,^3P^e4s\ ^4P^e$	5.10[−14]	$3d^6\,^3P^e4s\ ^4P^e$	1.62[−14]	$3d^6\,^3D^e4s\ ^4D^e$	2.93[−14]	$3d^6\,^3F^e4p\ ^4D^o$	3.04[−14]
$3d^6\,^5D^e4f\ ^4F^o$	4.65[−14]	$3d^6\,^5D^e5d\ ^4G^e$	1.58[−14]	$3d^6\,^3D^e4p\ ^4F^o$	2.59[−14]	$3d^6\,^5D^e4p\ ^4P^o$	2.77[−14]
Sum=	3.38[−12]		9.52[−13]		1.11[−12]		1.25[−12]
Total=	2.97[−11]		6.97[−12]		4.18[−12]		4.02[−12]
% contribution=	11%		14%		27%		31%

IV. CONCLUSION

Total and state-specific recombination rate coefficients for the recombined ion Fe II are obtained in the close coupling approximation employing a unified treatment. Present work represents a detailed study for the electron-ion recombination for Fe II. The total rates differ considerably from the currently used values higher in the low-temperature region, and are lower in the high-temperature region. Based on the atomic data for the photoionization cross sections and DR collision strengths, the total rates should be accurate to 10–30 %, except possibly at high temperatures (beyond 10^5 K) not of practical importance. The present recombination rates are necessary for accuracy and self-consistency in ionization balance between photoionization and recombination in photoionization models using the Opacity Project photoionization cross sections, which differ considerably from earlier works.

For further information regarding the state-selective recombination rate coefficients of all the low-n bound states of Fe II, see Ref. [17].

ACKNOWLEDGMENTS

I would like to thank Professor Anil K. Pradhan for contributions (supported by NSF grant for the Iron Project Grant No. PHY-9421898). This work was supported by NASA Grants No. NAGW-3315 and No. NAS-32643. The computational work was carried out on the Cray Y-MP at the Ohio Supercomputer Center.

[1] D.T. Woods, J.M. Shull, and C.L. Sarazin, Astrophys. J. **249**, 399 (1981).
[2] Y. Hahn, J. Quant. Spectrosc. Radiat. Transfer **41**, 315 (1989).
[3] S.N. Nahar and A.K. Pradhan, J. Phys. B **27**, 429 (1994).
[4] S.N. Nahar, Phys. Rev. A **53**, 1545 (1996).
[5] A. Burgess, Astrophys. J. **141**, 1588 (1965).
[6] S.N. Nahar and A.K. Pradhan, Phys. Rev. Lett. **68**, 1488 (1992).
[7] S.N. Nahar and A.K. Pradhan, Phys. Rev. A **49**, 1816 (1994).
[8] S.N. Nahar and A.K. Pradhan, Astrophys. J. **447**, 966 (1995).
[9] S.N. Nahar, Astrophys. J. Suppl. **101**, 423 (1995); **106**, 213 (1996).
[10] S.N. Nahar, Phys. Rev. A **53**, 2417 (1996).
[11] S.N. Nahar, M.A. Bautista, and A.K. Pradhan, Astrophys. J. (to be published).
[12] M.J. Seaton, J. Phys. B **20**, 6363 (1987); K.A. Berrington, P.G. Burke, K. Butler, M.J. Seaton, P.J. Storey, K.T. Taylor, and Yu. Yan, J. Phys. B **20**, 6379 (1987).
[13] D.G. Hummer, K.A. Berrington, W. Eissner, A.K. Pradhan, H.E. Saraph, and J.A. Tully, Astron. Astrophys. **279**, 298 (1993).
[14] R.H. Bell and M.J. Seaton, J. Phys. B **18**, 1589 (1985).
[15] V.L. Jacobs, J. Davis, P.C. Kepple, and M. Blaha, Astrophys. J. **211**, 605 (1977).
[16] M. Arnaud and J. Raymond, Astrophys. J. **398**, 395 (1992).
[17] The state-selective recombination rate coefficients of all the low-n bound states of Fe II may be obtained from the author via electronic address: nahar@seaton.mps.ohio-state.edu.